Biophysical Chemistry 171 (2013) 76–83

Contents lists available at SciVerse ScienceDirect

Biophysical Chemistry

journal homepage: http://www.elsevier.com/locate/biophyschem

# Parametrisation of the free energy of ATP binding to wild-type and mutant Kir6.2 potassium channels

Oscar Moran [a,*], Alessandro Grottesi [b], Andrew J. Chadburn [c], Paolo Tammaro [c,**]

[a] Istituto di Biofisica, CNR, Genova, Italy
[b] Computational Medicine and Biology Group, CASPUR, Roma, Italy
[c] Faculty of Life Sciences, University of Manchester, UK

## HIGHLIGHTS

- Structural homology models of wild-type and mutant Kir6.2 channels were developed.
- ATP binding free-energies were estimated with Linear Interaction Energy (LIE) method.
- Theoretically and experimentally determined ATP binding free energies were compared.
- This analysis leads to the identification of the conformation of ATP bound to Kir6.2.
- LIE parametrisation allows prediction of effects of Kir6.2 mutations on ATP affinity.

## GRAPHICAL ABSTRACT

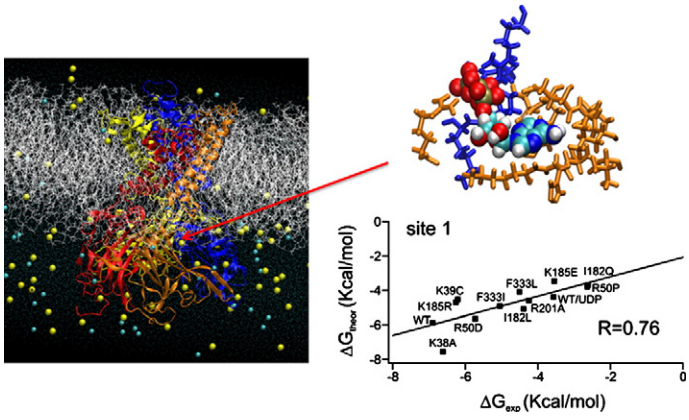


## ARTICLE INFO

*Article history:*
Received 5 October 2012
Received in revised form 30 October 2012
Accepted 30 October 2012
Available online 16 November 2012

*Keywords:*
ATP-sensitive potassium channel
Kir6.2
Molecular dynamics
Homology modelling
Linear Interaction Energy (LIE) method

## ABSTRACT

ATP-sensitive $K^+$ ($K_{ATP}$) channels, comprised of pore-forming Kir6.x and regulatory SURx subunits, play important roles in many cellular functions; because of their sensitivity to inhibition by intracellular ATP, $K_{ATP}$ channels provide a link between cell metabolism and membrane electrical activity. We constructed structural homology models of Kir6.2 and a series of Kir6.2 channels carrying mutations within the putative ATP-binding site. Computational docking was carried out to determine the conformation of ATP in its binding site. The Linear Interaction Energy (LIE) method was used to estimate the free-energy of ATP binding to wild-type and mutant Kir6.2 channels. Comparisons of the theoretical binding free energies for ATP with those determined from mutational experiments enabled the identification of the most probable conformation of ATP bound to the Kir6.2 channel. A set of LIE parameters was defined that may enable prediction of the effects of additional Kir6.2 mutations within the ATP binding site on the affinity for ATP.

Crown Copyright © 2012 Published by Elsevier B.V. All rights reserved.

* Correspondence to: O. Moran, Istituto di Biofisica, National Research Council, Italy. Tel.: +39 010 647 5550.
** Correspondence to: P. Tammaro, Faculty of Life Sciences, University of Manchester, UK. Tel.: +44 161 275 1703.
*E-mail addresses:* oscar.moran@cnr.it (O. Moran), paolo.tammaro@manchester.ac.uk (P. Tammaro).

## 1. Introduction

ATP-sensitive $K^+$ ($K_{ATP}$) channels are a class of ligand-gated channel that play a pivotal role in a multitude of cellular functions. The key

0301-4622/$ – see front matter. Crown Copyright © 2012 Published by Elsevier B.V. All rights reserved.
http://dx.doi.org/10.1016/j.bpc.2012.10.006

feature of $K_{ATP}$ channels is their sensitivity to inhibition by intracellular ATP with the half-maximal effect occurring in the micromolar range. Thus, $K_{ATP}$ channels provide a varying hyperpolarising force that forms a link between cellular metabolism and membrane electrical activity [1–4]. The quaternary structure of the $K_{ATP}$ channel involves four inwardly rectifying $K^+$ (Kir6.x) subunits assembled into a tetrameric pore and four sulphonylurea receptor (SURx) subunits surrounding the central pore structure [5–7]. Two isoforms of Kir6.x have been identified in mammals (Kir6.1 and Kir6.2) [8–11] with an additional isoform (Kir6.3) discovered in zebra fish [12]. Two SURx isoforms exist (SUR1 and SUR2) and further differentiation arises from alternative splicing of SUR2 into SUR2A and SUR2B [11,13–15]. Both Kir6.x and SURx are involved in metabolic regulation of the channel. Binding of ATP (or ADP) to Kir6.x inhibits the channel [16,17], while interaction of MgATP or MgADP with SURx enhances channel activity [18–20]. Thus, the $K_{ATP}$ channel represents a unique case of a ligand-gated channel that is both inhibited and activated by the same type of ligands. Overall, the inhibitory effects of nucleotides on channel activity prevail over their activating effects: an increase in the intracellular concentration of MgATP results in a decrease in channel activity. An indication of the physiological relevance of the Kir6.2 inhibitory site is the fact that mutations in this region result in human diseases such as neonatal diabetes (reviewed in [21]).

Homology modelling has been invaluable for the identification of residues forming the inhibitory ATP-binding site. Structural models of the isolated C-terminal domain [22,23] or transmembrane domains [24,25] of Kir6.2 as well as a model of the full-length Kir6.2 [26] have been previously generated. The ATP binding-site identified by Antcliff and collaborators [26] via molecular docking methods appeared to involve residues from both the N- and C-terminal domains of Kir6.2. The proposed location of the ATP-binding site was consistent with all previous mutational experiments that identified residues involved in ATP binding [16,22,27–30].

The study presented here aims to further our understanding of the mechanism of nucleotide binding to Kir6.2 channels. An approach similar to the one adopted by Antcliff and co-workers [26] was utilised to derive a homology model of Kir6.2 involving new structural templates that have become available during the intervening period. These new templates present higher structural resolution and have greater sequence homology with Kir6.2 compared to those that were previously available. Computational docking was used to define the ATP binding site in this model. Additionally, models were constructed for a series of Kir6.2 mutants with a known degree of ATP-sensitivity. Comparisons of the theoretical binding free energies ($\Delta G$) for ATP with the $\Delta G$ calculated from mutational experiments enabled the identification of the most probable conformation of ATP docked to the Kir6.2 inhibitory site. A set of parameters were obtained that may allow prediction of the effects of additional Kir6.2 mutations on the binding of ATP (or of other nucleotides) and may help in understanding the differential ATP-sensitivity presented by the various Kir6.x isoforms.

## 2. Methods

### 2.1. Homology modelling of wild-type and mutant Kir6.2 channels

Templates for Kir6.2 (UniProtKB P70673) were selected based on sequence homology with channels of known structure. Templates used include: the intracellular domain of mouse Kir3.1 (PDB 1N9P), chicken Kir2.2 (PDB 3JYC) and chimeric mouse Kir3.1/KirBac1.3 (PDB 2QKS). The program Modeler 9.8 [31] was used to generate 50 models with an overall root mean square deviation (RMSD) $\leq$ 4.0 Å. Models presenting more than 10% of residues outside the allowed region of the Ramachandran plot were discarded. Among the remaining models, the one associated with the highest Modeller scoring function and the lowest average RMSD of alpha carbons (Cα) relative to the templates was selected for further study. The complete Kir6.2 channel was modelled as a tetramer.

### 2.2. Energy minimisation and molecular dynamics

Energy minimisation and molecular dynamics (MD) were performed with the program NAMD [32] using the Charmm27 force field. A first energy minimisation was performed to remove the gross molecule errors. Subsequently, the model was inserted into a lipid membrane and hydrated using the routines available in VMD [33]. A 1-palmitoyl-2-oleoyl-sn-glycero-3-phosphocholine (POPC) bilayer of 130 × 130 Å was used while the two sides of the bilayer were solvated with standard TIP3 water molecules. Sodium and chloride ions corresponding to a concentration of 100 mM were included in the water phase to neutralise the charges of the system. The system was extensively minimised by restraining protein heavy atoms and allowing water molecules to equilibrate the protein–solvent interactions. The system was heated to 300 K in a stepwise manner at a constant pressure of 1 atm. A MD simulation at 300 K was run for 10 ns to equilibrate the system. The calculation interval for the equations of motion was 2 fs. Long-range electrostatic interactions were calculated using the Ewald approximation using periodic boxes. The box side was at least at 20 Å apart from the protein atoms. The SHAKE [34] procedure was employed to constrain all bonds connecting hydrogen atoms. Non-bonded energy terms were calculated with smoothing cut-off functions to both the electrostatics and van der Waals forces, starting at 10 Å, to a complete cut-off at 12 Å. The Ewald sum was computed using the Particle-Mesh Ewald (PME) method as implemented in the NAMD program [32]. This implementation is a fast numerical method to compute the Ewald sum that uses the smooth PME (SPME) [35] method for full electrostatic computations. The maximum space between grid points was 1 Å. The cost of PME is proportional to N log N and the time reduction is significant even for a small system of several hundred atoms.

All analyses were performed using Gromacs [36], VMD and self-written software.

Kir6.2 mutants were generated by using the routine Mutator implemented in the VMD program. Eleven mutations, for which the experimentally determined concentration of ATP causing half-maximal inhibition ($IC_{50}$) was known, were considered. Each mutation was introduced, one at a time, in each subunit of the Kir6.2 tetramer, with the ATP molecules bound as described below. An additional model in which UDP, instead of ATP, was bound to Kir6.2 was also constructed. For each mutant channel, energy minimisation, insertion into a POPC bilayer, hydration and addition of sodium and chloride to neutralise the charges were conducted as described above.

### 2.3. Docking of ATP

Preparation of the data, including addition of hydrogens to the ligand and the receptor, determination of the rotatable bonds, partial charge distribution (via the Gasteiger method), definition of the region of Kir6.2 in which to execute the docking and the grid calculation for the docking algorithms were done with the AutoDockTools 1.5.4 program [37]. The receptor molecule was the Kir6.2 model, minimised and equilibrated as indicated above.

The docking of ATP to Kir6.2 was guided by experimental data that highlighted a set of residues that participate in the ATP binding site. These residues include: K38 [28], K39 [28,29,38], R50 [28,29,38], I182 [16,22,23,39], K185 [29], R201 [30,38], and F333 [40]. The active site radius was set at 6.5 Å from these residues.

Docking of ATP was done using the Lamarckian Genetic Algorithm protocol implemented in Autodock 4.2 [37]. A total of 200 runs were carried out to obtain 200 different configurations of ATP bound to the Kir6.2 binding site. To obtain a large number of different conformations of bound ATP, only runs that resulted in an RMS difference > 2 Å were considered. During the docking procedure, all rotatable bonds in

the ATP molecule were allowed to rotate. ATP conformations that were >6.5 Å away from the residues forming the putative binding site were rejected. Finally, the four ATP-binding conformations with the highest docking score, one for each of the four putative binding sites, were selected. These conformations were called site 1, site 2, site 3 and site 4.

### 2.4. Binding free energy calculations

The free energy of binding, $\Delta G_{bind}$, was evaluated for each of the four ATP (or UDP) molecules bound to Kir6.2 using the linear integration of energy method (LIE; [41–44]). LIE is based on evaluation of ligand interaction energetics in the bound and free states. Therefore, two MD simulations were carried out, one with ATP free in solution and one where ATP was bound to the solvated receptor, and averages of the interaction energies between the ligand and its surroundings were evaluated. The binding free energy was obtained from these averages as:

$$\Delta G_{bind} \simeq \Delta G^{(nonpolar)} + \Delta G^{(polar)} = \alpha\left(\left\langle V_{l-s}^{vdw}\right\rangle_{bound} - \left\langle V_{l-s}^{(vdw)}\right\rangle_{free}\right) + \beta\left(\left\langle V_{l-s}^{(ele)}\right\rangle_{bound} - \left\langle V_{l-s}^{(ele)}\right\rangle_{free}\right) + \gamma \quad (1)$$

where ⟨⟩ denotes MD averages of the non-bonded van der Waals (*vdw*) and electrostatic (*ele*) interactions between the ligand (ATP) and its surrounding environment (*l–s*), i.e. either the solvated receptor binding site (*bound*) or just the solvent (*free*). The parameters of this equation are the weight coefficients $\alpha$ and $\beta$ for the non-polar and polar binding energy contributions, respectively, and an additional constant $\gamma$.

Energy terms for the binding free energy calculations were obtained from the MD simulations applied on a restricted region of the system. A free (non-restrained) MD was carried out in a sphere of 18 Å radius around each of the four ATP molecules bound to the protein. A buffer shell of 5 Å, with a harmonic restraint of 5 kcal/mol Å, was defined around the active region. This shell was further surrounded by an additional 5 Å shell with a harmonic restraint of 50 kcal/mol Å. All atoms outside this external shell were tightly restrained throughout the entire simulation. All simulations were carried out using NAMD and with the Charmm27 parameter forcefield. Data were sampled from MD simulations of >5 ns that were run for each model after the initial 10 ns equilibration. In this region of the trajectory the simulation is already stable, as observed from the RMSD. The average RMSD obtained after the initial 10 ns equilibration for all simulations was between 0.62 and 0.67 Å, with a fluctuation of about 3% in the sampling window of the trajectory.

## 3. Results

### 3.1. Homology modelling

Three templates were used for the construction of the model. The sequence of Kir6.2, from residue 29 to residue 356, has 50% and 43% identity to mouse Kir3.1/KirBac1.3 (2QKS) and chicken Kir2.2 (3JYC), respectively. These structures were used to construct the proximal N- and C-terminal domains as well as the transmembrane domains of Kir6.2. The sequence of the intracellular domains of mouse Kir3.1 (1N9P) has 55% identity between residues 30 and 49 and 50% between residues 177 and 351 of Kir6.2 and it was therefore used to model the distal N- and C-termini of the channel. Fig. 1A shows a sequence alignment of the template structures described above and Kir6.2.

The complete, assembled and energy minimised Kir6.2 tetrameric model had a total length of ~122 Å along the axis perpendicular to the membrane and a maximal width of 80 Å. The four Kir6.2 subunits, each composed of 2 transmembrane (TM) domains, co-assembled to form a central pore that hosts the selectivity filter region (Fig. 1B). The pore was 5.6 Å at the widest part and 1.7 Å within the selectivity filter. A large (~86 Å×87 Å) cytoplasmic domain was also modelled, harbouring the ATP-binding site. The stability of the model was evaluated by running a short MD simulation in the presence of a POPC membrane and explicit water molecules. The root mean square deviation (RMSD), after 5 ns, of the Cα atoms with respect to the original template structure was 0.29 nm, suggesting that the overall folding of Kir6.2 was stable.

### 3.2. Docking of ATP and free energy calculations

The four ATP-binding conformations with the highest docking score are shown in Fig. 2. We estimated $\Delta G_{bind}$ for ATP for each of the four docking conformations. Calculations were carried out for wild-type as well as for mutant channels. Also, $\Delta G_{bind}$ was calculated for UDP (rather than ATP) bound to wild-type Kir6.2. The van der Waals and electrostatic energies of the interaction between the nucleotide and its surroundings were expressed as the average of data calculated during a >5 ns trajectory (>2500 data points). Only data that were homogeneous, i.e. for which the distribution followed a single normal distribution, and for which the standard deviation of each energy term along the trajectory varied by less than 5%, were averaged. Table 1 shows the van der Waals ($\Delta V_{l-s}^{(vdw)}$) and electrostatic ($\Delta V_{l-s}^{(ele)}$) terms of the energy difference between the free and bound ATP calculated for wild-type and mutant Kir6.2 channels.

The $\Delta G_{bind}$ was calculated using Eq. (1). Note that the parameters $\alpha$, $\beta$ and $\gamma$ in Eq. (1) depend on the physical–chemical characteristics of the ligand and the binding site, as well as the forcefield used to evaluate the energy terms [41–50]. Therefore, to establish the numerical values for these parameters, experimental data obtained for different Kir6.2 mutants and from the substitution of ATP with UDP were considered. A set of Kir6.2 mutants for which the measured sensitivity to ATP spans approximately three orders of magnitude were used.

An approximation of the Gibbs free energy of binding calculated for these Kir6.2 mutants ($\Delta G_{exp}$) was defined as [51,52]:

$$\Delta G_{\exp} = RT \ln\left(\frac{IC_{50}}{1\mathrm{M}}\right) \quad (2)$$

where $IC_{50}$ is the dose causing half-maximal inhibition of the $K_{ATP}$ current, $R$ is the gas constant and $T$ is the absolute temperature.

The parameters $\alpha$, $\beta$ and $\gamma$ were obtained by fitting $\Delta G_{exp}$ with a multiparametric expression obtained substituting $\Delta G_{bind}$ in Eq. (1) as:

$$\Delta G_{\exp} = \alpha \Delta V_{l-s}^{vdw} + \beta \Delta V_{l-s}^{ele} + \gamma. \quad (3)$$

This procedure was applied to the data calculated for each of the four binding sites in the model. This analysis yielded values of $\alpha$, $\beta$ and $\gamma$ of 0.500, 1.0387 and 4.173, with $\chi^2$ of 11.01 for site 1; 0.355, 0.424 and −1.422 with $\chi^2$ of 52.10 for site 2; 0.470, −0.756 and 3.348, with $\chi^2$ of 87.52 for site 3; and 0.486, 0.060 and 0.306, with $\chi^2$ of 28.26 for site 4.

Table 2 includes the theoretical free energy of binding, $\Delta G_{theor}$, calculated using the parameters obtained above. These data were plotted versus $\Delta G_{exp}$ for each conformation of ATP in site 1 to site 4 (Fig. 3). The continuous lines in Fig. 3 represent linear regression fits of the data with correlation coefficients of 0.757, 0.055, 0.082 and 0.317 for sites 1, 2, 3 and 4, respectively (see Table 2). Notice that for sites 2 and 3 the slope is very low (0.06 and 0.12, respectively) and not statistically different from zero. In contrast, the slope of the regression of theoretical and experimental data for site 1 was positive and had a correlation coefficient higher than those of the other

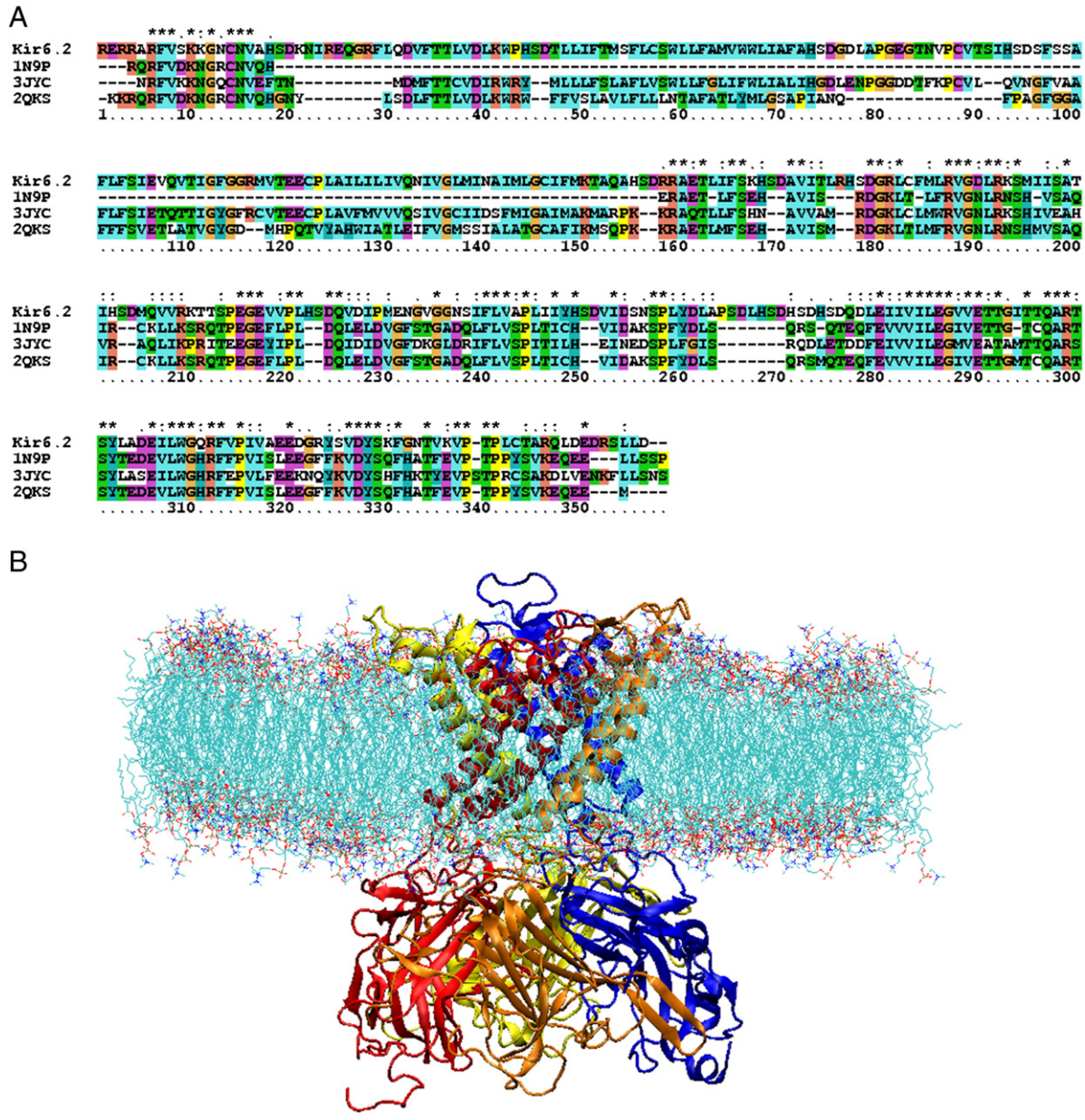


**Fig. 1.** A: Sequence alignment of template structures used for building the homology model of Kir6.2. Fully conserved residues are indicated with an asterisk; amino acids are coloured according to their type (ClustalX standard colors). B: Homology model of Kir6.2, represented as ribbons and coloured according to chain ID; POPC membrane is shown as lines. Water is omitted.

sites. This analysis indicates that the most probable conformation of ATP bound to Kir6.2 is the one assumed in site 1.

### 3.3. Residues interacting with ATP

In the model, residues that make close contacts with ATP in site 1, i.e. those presenting the centre of mass of their side chain within 4.5 Å of ATP, include: R50, R54, Q179, I182, F183, and K185 in one subunit and K38 and K39 in the adjacent subunit. Non-bonded intermolecular interactions (hydrogen bonding and salt bridges mediated by ion-pairs) between the ATP and surrounding residues in the binding pocket were analysed. We considered that a hydrogen bond between ATP and the channel residues occurred when the donor–acceptor distance was less than 3.5 Å and its occurrence during a 5 ns MD simulation lasted for at least 66% of the simulation time. A salt bridge was defined when two oxygen–nitrogen ion-pairs were within 3.2 Å for at least 66% of the simulation. Residues K39, R50 and R54 formed H-bonds with the phosphoryl moiety of ATP. Residues K38, K39, R50 and K185 were found to form salt bridges with the ATP phosphate moieties (Fig. 4). No oxygen–oxygen ion pairs were detected during the simulation.

## 4. Discussion

The aim of this work was to generate a structural model of ATP bound to its binding site in wild-type and mutant Kir6.2 channels that was quantitatively consistent with the experimentally determined degree of sensitivity to ATP observed for those channels. The first step to define the potential geometry of ATP in its binding pocket was therefore to develop a model of the Kir6.2 channel. To generate a complete model

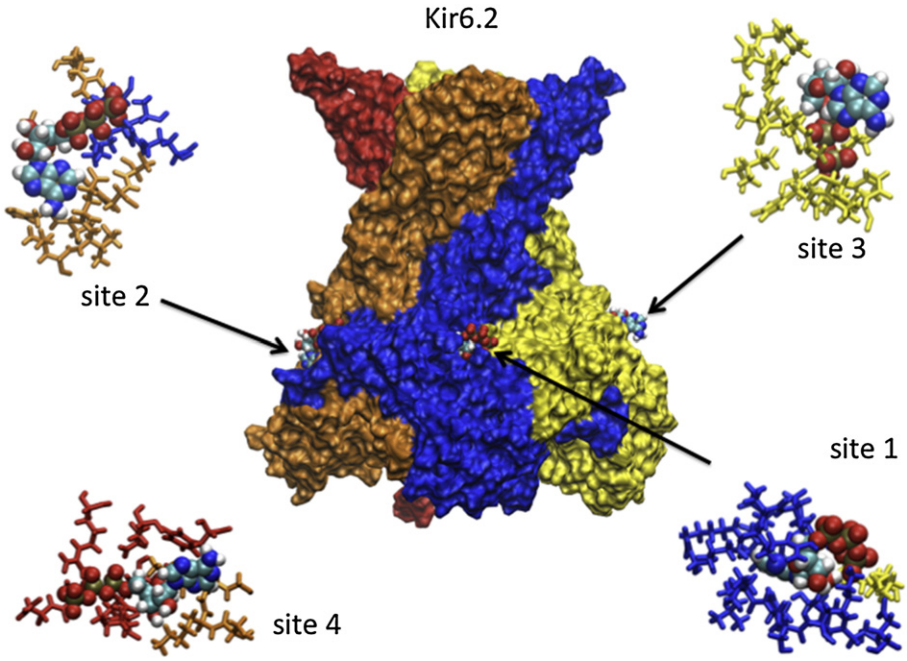


**Fig. 2.** Solid solvent accessible surface representation (centre) of Kir6.2 homology model with differently coloured monomers. Docked ATP molecules are represented as Van der Waals spheres. Close-up views of the individual binding sites for the four ATP (site 1 to site 4) are also shown. In the close-ups, only residues within 4.5 Å of the ATP molecule are shown and coloured according to different monomers.

of Kir6.2 we took an approach similar to the one used in Antcliff and collaborators [26]. The homology model obtained by Antcliff and collaborators [26] was based on the X-ray crystal structures of KirBac1.1 [53] and the intracellular domains of Kir3.1 [54]. The templates in the current study, in addition to the intracellular domains of Kir3.1 [54], were: chicken Kir2.2 [55] and chimeric mouse Kir3.1/KirBac1.3 [56]. These structures have a higher resolution (3.11 Å and 2.2 Å, respectively) than KirBac1.1 (3.65 Å). The sequence identity between Kir6.2 and KirBac1.1 is lower (~28%) than that between Kir6.2 and the sequence of the templates used here (~43–50%). Nevertheless, the similarity of the general topology of the previously generated model [26] with the model presented here is striking. Particularly, many residues that we identified to be involved in ATP binding are also in close proximity to ATP in the previous model. These include residues R50, I182, R201 and F333, which are mutated in permanent neonatal diabetes [21].

Molecular docking of ATP was executed by using a geometric matching/shape complementarity method implemented in AutoDock. This method accounts for the complementarity between the surfaces of the ligand and the receptor [37,57,58]. The main limitation of this method is that it cannot fully account for the fluctuations in the ligand or protein conformations, even when the rotatable bonds of the ligand were allowed to rotate. Therefore, the results of this docking are not deterministic and are subject to a high false-positive rate. To obtain a plausible conformation of the docked ATP in its binding site, the four best docking conformations, based on the scoring function used by the AutoDock program, were selected. Two other criteria were then used

**Table 1**

Hydrophobic ($\Delta V_{l-s}^{vdw} = \left\langle V_{l-s}^{vdw} \right\rangle_{bound} - \left\langle V_{l-s}^{vdw} \right\rangle_{free}$) and electrostatic energy ($\Delta V_{l-s}^{ele} = \left\langle V_{l-s}^{ele} \right\rangle_{bound} - \left\langle V_{l-s}^{ele} \right\rangle_{free}$) terms for the four proposed ATP binding conformations (see text for details). Data were obtained for the wild type (WT) Kir6.2 channel, for 11 point mutations of Kir6.2 channels and for a Kir6.2 channel where ATP was substituted by UDP. Values represent the difference of the averages ± the standard deviation of the difference.

| | Site 1 | | Site 2 | | Site 3 | | Site 4 | |
|---|---|---|---|---|---|---|---|---|
| | $\Delta V_{l-s}^{vdw}$ (kcal/mol) | $\Delta V_{l-s}^{ele}$ (kcal/mol) | $\Delta V_{l-s}^{vdw}$ (kcal/mol) | $\Delta V_{l-s}^{ele}$ (kcal/mol) | $\Delta V_{l-s}^{vdw}$ (kcal/mol) | $\Delta V_{l-s}^{ele}$ (kcal/mol) | $\Delta V_{l-s}^{vdw}$ (kcal/mol) | $\Delta V_{l-s}^{ele}$ (kcal/mol) |
| WT | −23.1 ± 3.1 | 1.5 ± 1.1 | −13.2 ± 3.4 | 2.2 ± 1.2 | −19.2 ± 3.2 | 2.0 ± 1.2 | −16.7 ± 3.2 | 1.8 ± 1.1 |
| K38A | −20.3 ± 3.2 | −1.5 ± 1.4 | −4.3 ± 3.3 | −3.2 ± 1.1 | −14.6 ± 3.3 | −0.1 ± 1.2 | −8.9 ± 3.2 | −2.0 ± 1.2 |
| K39C | −16.8 ± 3.2 | −0.3 ± 1.2 | −4.1 ± 3.3 | −2.5 ± 1.2 | −16.5 ± 3.3 | −0.2 ± 1.1 | −9.1 ± 3.2 | −0.9 ± 1.3 |
| R50D | −19.6 ± 3.2 | 0.0 ± 1.1 | −5.0 ± 3.3 | −3.2 ± 1.1 | −8.6 ± 3.4 | −0.1 ± 1.2 | −8.0 ± 3.2 | 0.3 ± 1.3 |
| R50P | −15.1 ± 3.2 | −0.4 ± 1.1 | 0.3 ± 3.3 | −0.8 ± 1.3 | −11.3 ± 3.2 | 0.4 ± 1.3 | −8.2 ± 3.3 | −1.2 ± 1.3 |
| I182Q | −16.9 ± 3.2 | 0.6 ± 1.2 | −7.0 ± 3.2 | −2.8 ± 1.1 | −17.9 ± 3.3 | −0.4 ± 1.2 | −10.1 ± 3.2 | −3.2 ± 1.1 |
| I182L | −18.5 ± 3.2 | 0.0 ± 1.1 | −4.5 ± 3.3 | −2.3 ± 1.2 | −14.4 ± 3.3 | −0.5 ± 1.1 | −10.5 ± 3.3 | −2.2 ± 1.2 |
| K185E | −16.4 ± 3.2 | 0.6 ± 1.3 | −6.2 ± 3.3 | −3.0 ± 1.1 | −18.2 ± 3.3 | −0.6 ± 1.1 | −8.6 ± 3.2 | −1.6 ± 1.3 |
| K185R | −16.9 ± 3.4 | −0.4 ± 1.2 | −6.5 ± 3.2 | −3.6 ± 1.1 | −20.2 ± 3.2 | 0.2 ± 1.2 | −11.5 ± 3.2 | −2.8 ± 1.3 |
| R201A | −19.4 ± 3.1 | 0.9 ± 1.2 | −6.5 ± 3.2 | −3.3 ± 1.1 | −13.9 ± 3.3 | −0.4 ± 1.1 | −11.7 ± 3.3 | −1.8 ± 1.2 |
| F333I | −15.9 ± 3.3 | −1.1 ± 1.2 | −1.0 ± 3.3 | −1.5 ± 1.3 | −17.0 ± 3.2 | −0.9 ± 1.2 | −8.9 ± 3.2 | −2.6 ± 1.1 |
| F333L | −16.2 ± 3.2 | −0.2 ± 1.2 | −3.7 ± 3.3 | −1.1 ± 1.2 | −17.9 ± 3.3 | −1.3 ± 1.1 | −8.5 ± 3.3 | −2.3 ± 1.2 |
| WT/UDP | −20.0 ± 3.5 | 1.4 ± 1.2 | −15.3 ± 3.2 | −2.2 ± 1.0 | −26.0 ± 3.2 | −0.5 ± 1.0 | −11.4 ± 3.3 | −0.6 ± 1.6 |

**Table 2**
Theoretical free energy of binding, $\Delta G_{theor}$, obtained after the parametrisation of data in Table 1 using Eq. (1). Values of experimental free energy of binding, $\Delta G_{exp}$, were calculated from the $IC_{50}$ values according to Eq. (2). The results of the linear regression of $\Delta G_{theor}$ vs $\Delta G_{exp}$ for each putative site, as shown in Fig. 3, are shown below, where *a* represents the intercept, *b* is the slope, and *r* is the correlation coefficient.

| | Site 1 | Site 2 | Site 3 | Site 4 | | | |
|---|---|---|---|---|---|---|---|
| | $\Delta G_{theor}$ (kcal/mol) | $\Delta G_{theor}$ (kcal/mol) | $\Delta G_{theor}$ (kcal/mol) | $\Delta G_{theor}$ (kcal/mol) | $IC_{50}$ (μM) | $\Delta G_{exp}$ (kcal/mol) | |
| WT | −5.88 | −5.19 | −7.21 | −7.71 | 9.4 | −6.90 | [a] |
| K38A | −7.56 | −4.34 | −3.45 | −4.14 | 15 | −6.62 | [28] |
| K39C | −4.54 | −3.96 | −4.28 | −4.15 | 30 | −6.21 | [30] |
| R50D | −5.66 | −4.55 | −0.62 | −3.58 | 67 | −5.73 | [29] |
| R50P | −3.78 | −1.67 | −2.26 | −3.73 | 12,000 | −2.64 | [29] |
| I182Q | −3.68 | −5.11 | −4.76 | −4.80 | 12,250 | −2.62 | [16,39] |
| I182L | −5.08 | −4.00 | −3.07 | −4.92 | 620 | −4.40 | [23,39] |
| K185E | −3.46 | −4.92 | −4.78 | −3.98 | 2600 | −3.55 | [29] |
| K185R | −4.70 | −5.28 | −6.35 | −5.45 | 27.5 | −6.26 | [29] |
| R201A | −4.60 | −5.17 | −2.92 | −5.51 | 820 | −4.25 | [30,60] |
| F333I | −4.91 | −2.41 | −3.94 | −4.17 | 208 | −5.05 | [40] |
| F333L | −4.09 | −3.23 | −4.10 | −3.99 | 510 | −4.51 | [a] |
| WT/UDP | −4.39 | −7.80 | −8.46 | −5.28 | 2500 | −3.57 | [a] |
| a | −2.07 | −4.16 | −3.76 | −3.57 | | | |
| b | 0.57 | 0.06 | 0.12 | 0.24 | | | |
| r | 0.76 | 0.05 | 0.08 | 0.32 | | | |

[a] Chadburn and Tammaro, unpublished results.

to identify, among these four conformations, the one that may more closely reflect the true conformation assumed by ATP in its binding site in Kir6.2. The first was to assume that residues known to be involved in determining the sensitivity of Kir6.2 channels to ATP, based on published electrophysiological data, are in close proximity to the docked ATP molecule. Residues that were taken into account were K38, K39, R50, I182, K185, R201 and F333. Mutations in these residues give rise to channels with impaired sensitivity to ATP while maintaining unaltered, ligand-independent channel gating suggesting that they form part of the binding site [59] and that their effect on the channel's ATP-sensitivity is not secondary to a change in channel gating. Other residues have been shown to alter ATP sensitivity but their mechanisms of action appear to be indirect i.e. secondary to an increase in the open probability of the channel rather than affecting ATP binding [4,21]. The second selection criteria were based on $\Delta G$ calculations. Thus, $\Delta G$ from the electrostatic and van der Waals energy contributions were calculated from molecular dynamics trajectories for different Kir6.2 mutants using the LIE method. The correlation between the theoretical $\Delta G$ calculated in

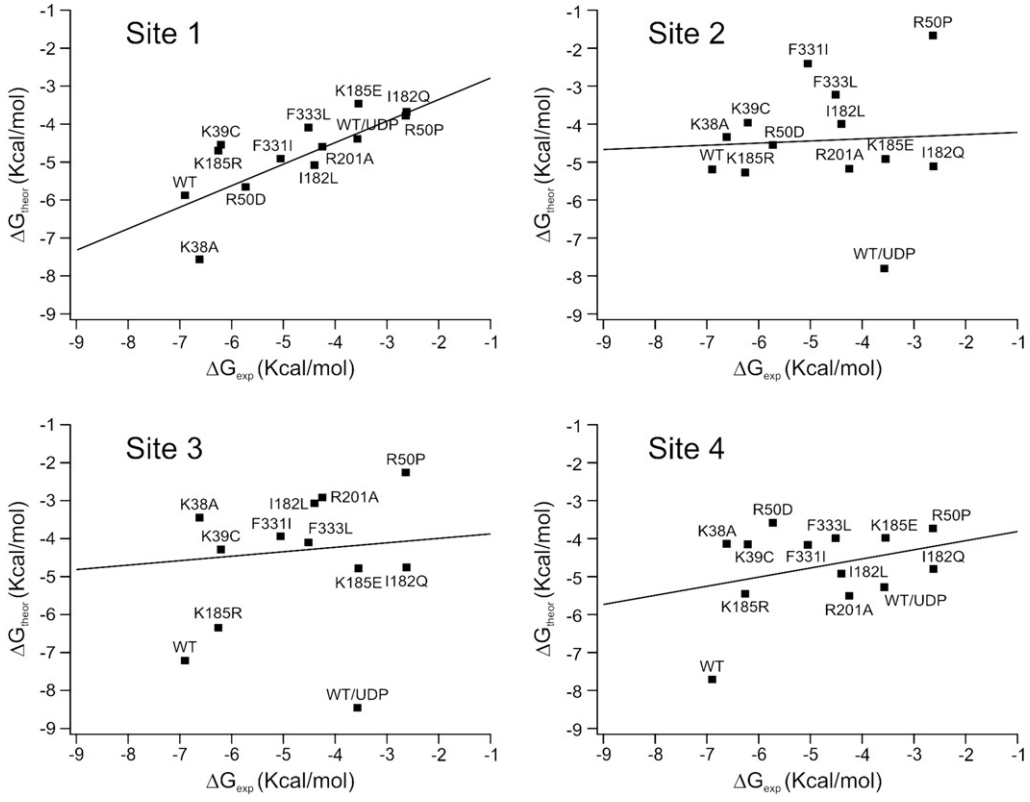


**Fig. 3.** $\Delta G_{theor}$ versus $\Delta G_{exp}$ for the wild-type and mutant Kir6.2 channels. Straight lines represent the best fits to the data using equation 3.

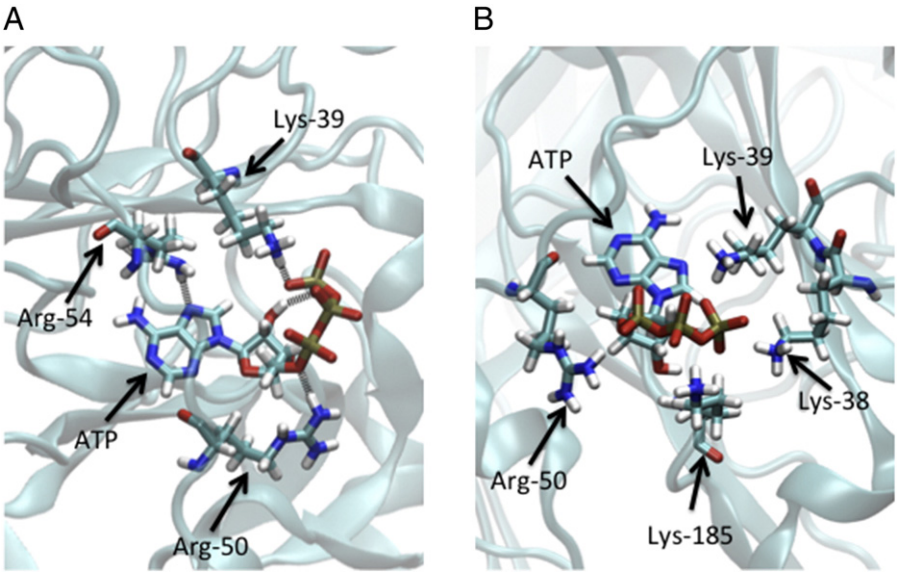


**Fig. 4.** A, Close-up view of "site 1" binding pocket of Kir6.2 with ATP bound. Residues forming hydrogen bonds with ATP are represented as sticks. B, Residues forming ions-pairs with ATP are shown as sticks. In both A and B channel atoms not involved in interactions are shown as ribbons.

this way and the $\Delta G$ estimated from measured $IC_{50}$ values was best for the ATP conformation assumed in site 1. Therefore, this conformation was considered the most plausible image of the ATP bound to Kir6.2.

Importantly, determination of the numerical values for the constants $\alpha$, $\beta$ and $\gamma$ of Eq. (1) could be used to make predictions of the functional effects of new mutations at the ATP-binding site on the ATP-sensitivity of Kir6.2 or to understand the mechanism of ATP-sensitivity of other Kir6.x channels. For example, Kir6.1 shares ~70% sequence homology with Kir6.2 but it is about 20-fold less sensitive to ATP inhibition [38]. The sequences of the putative ATP-binding sites of Kir6.1 and Kir6.2 are conserved with the exception of K39 (S40 in Kir6.1) and K185 (R195 in Kir6.1). It will be interesting to determine if these substitutions in the model predict a change in ATP affinity and if experimentally these substitutions alter the sensitivity of Kir6.2 channel to ATP.

## Acknowledgements

P.T. holds a Research Council (RCUK) Fellowship. This work was supported by a CASPUR (gpu11-905) grant to O.M. and a BBSRC (BB/H000259/1) grant to P.T.

## Appendix A. Supplementary data

Supplementary data to this article can be found online at http://dx.doi.org/10.1016/j.bpc.2012.10.006.

## References

[1] J. Bryan, W.H. Vila-Carriles, G. Zhao, A.P. Babenko, L. Aguilar-Bryan, Toward linking structure with function in ATP-sensitive $K^+$ channels, Diabetes 53 (Suppl. 3) (2004) S104–S112.
[2] G.C. Kane, X.K. Liu, S. Yamada, T.M. Olson, A. Terzic, Cardiac $K_{ATP}$ channels in health and disease, Journal of Molecular and Cellular Cardiology 38 (2005) 937–943.
[3] J.S. McTaggart, R.H. Clark, F.M. Ashcroft, The role of the $K_{ATP}$ channel in glucose homeostasis in health and disease: more than meets the islet, Journal of Physiology (London) 588 (2010) 3201–3209.
[4] C.G. Nichols, $K_{ATP}$ channels as molecular sensors of cellular metabolism, Nature 440 (2006) 470–476.
[5] J.P. Clement, K. Kunjilwar, G. Gonzalez, M. Schwanstecher, U. Panten, L. Aguilar-Bryan, J. Bryan, Association and stoichiometry of $K_{ATP}$ channel subunits, Neuron 18 (1997) 827–838.
[6] S. Shyng, C.G. Nichols, Octameric stoichiometry of the $K_{ATP}$ channel complex, Journal of General Physiology 110 (1997) 655–664.
[7] M.V. Mikhailov, J.D. Campbell, H. de Wet, K. Shimomura, B. Zadek, R.F. Collins, M.S.P. Sansom, R.C. Ford, F.M. Ashcroft, 3-D structural and functional characterization of the purified KATP channel complex Kir6.2-SUR1, EMBO Journal 24 (2005) 4166–4175.
[8] N. Inagaki, Y. Tsuura, N. Namba, K. Masuda, T. Gonoi, M. Horie, Y. Seino, M. Mizuta, S. Seino, Cloning and functional characterization of a novel ATP-sensitive potassium channel ubiquitously expressed in rat tissues, including pancreatic islets, pituitary, skeletal muscle, and heart, Journal of Biological Chemistry 270 (1995) 5691–5694.
[9] H. Sakura, C. Ammälä, P.A. Smith, F.M. Gribble, F.M. Ashcroft, Cloning and functional expression of the cDNA encoding a novel ATP-sensitive potassium channel subunit expressed in pancreatic beta-cells, brain, heart and skeletal muscle, FEBS Letters 377 (1995) 338–344.
[10] N. Inagaki, T. Gonoi, J.P. Clement IV, N. Namba, J. Inazawa, G. Gonzalez, L. Aguilar-Bryan, S. Seino, J. Bryan, Reconstitution of $IK_{ATP}$: an inward rectifier subunit plus the sulfonylurea receptor, Science 270 (1995) 1166–1170.
[11] S. Isomoto, C. Kondo, M. Yamada, S. Matsumoto, O. Higashiguchi, Y. Horio, Y. Matsuzawa, Y. Kurachi, A novel sulfonylurea receptor forms with BIR (Kir6.2) a smooth muscle type ATP-sensitive $K^+$ channel, Journal of Biological Chemistry 271 (1996) 24321–24324.
[12] C. Zhang, T. Miki, T. Shibasaki, M. Yokokura, A. Saraya, S. Seino, Identification and characterization of a novel member of the ATP-sensitive $K^+$ channel subunit family, Kir6.3, in zebrafish, Physiological Genomics 24 (2006) 290–297.
[13] N. Inagaki, T. Gonoi, J.P. Clement, C.Z. Wang, L. Aguilar-Bryan, J. Bryan, S. Seino, A family of sulfonylurea receptors determines the pharmacological properties of ATP-sensitive $K^+$ channels, Neuron 16 (1996) 1011–1017.
[14] A. Morrissey, E. Rosner, J. Lanning, L. Parachuru, P. Dhar Chowdhury, S. Han, G. Lopez, X. Tong, H. Yoshida, T.Y. Nakamura, M. Artman, J.P. Giblin, A. Tinker, W.A. Coetzee, Immunolocalization of KATP channel subunits in mouse and rat cardiac myocytes and the coronary vasculature, BMC Physiology 5 (2005) 1.
[15] P. Tammaro, P. Proks, F.M. Ashcroft, Functional effects of naturally occurring KCNJ11 mutations causing neonatal diabetes on cloned cardiac $K_{ATP}$ channels, Journal of Physiology (London) 571 (2006) 3–14.
[16] P. Drain, L. Li, J. Wang, $K_{ATP}$ channel inhibition by ATP requires distinct functional domains of the cytoplasmic c terminus of the pore-forming subunit, Proceedings of the National Academy of Sciences of the United States of America 95 (1998) 13953–13958.
[17] S.J. Tucker, F.M. Gribble, C. Zhao, S. Trapp, F.M. Ashcroft, Truncation of Kir6.2 produces ATP-sensitive $K^+$ channels in the absence of the sulphonylurea receptor, Nature 387 (1997) 179–183.
[18] C.G. Nichols, S.L. Shyng, A. Nestorowicz, B. Glaser, J.P. Clement IV, G. Gonzalez, L. Aguilar-Bryan, M.A. Permutt, J. Bryan, Adenosine diphosphate as an intracellular regulator of insulin secretion, Science 272 (1996) 1785–1787.
[19] M. Matsuo, K. Tanabe, N. Kioka, T. Amachi, K. Ueda, Different binding properties and affinities for ATP and ADP among sulfonylurea receptor subtypes, SUR1, SUR2A, and SUR2B, Journal of Biological Chemistry 275 (2000) 28757–28763.
[20] L.V. Zingman, A.E. Alekseev, M. Bienengraeber, D. Hodgson, A.B. Karger, P.P. Dzeja, A. Terzic, Signaling in channel/enzyme multimers: ATPase transitions in SUR module gate ATP-sensitive $K^+$ conductance, Neuron 31 (2001) 233–245.
[21] F.M. Ashcroft, ATP-sensitive potassium channelopathies: focus on insulin secretion, The Journal of Clinical Investigation 115 (2005) 2047–2058.
[22] S. Trapp, S. Haider, P. Jones, M.S.P. Sansom, F.M. Ashcroft, Identification of residues contributing to the ATP binding site of Kir6.2, EMBO Journal 22 (2003) 2903–2912.
[23] L. Li, X. Geng, M. Yonkunas, A. Su, E. Densmore, P. Tang, P. Drain, Ligand-dependent linkage of the ATP site to inhibition gate closure in the $K_{ATP}$ channel, Journal of General Physiology 126 (2005) 285–299.

[24] C.E. Capener, P. Proks, F.M. Ashcroft, M.S. Sansom, Filter flexibility in a mammalian K channel: models and simulations of Kir6.2 mutants, Biophysical Journal 84 (2003) 2345–2356.
[25] G. Loussouarn, E.N. Makhina, T. Rose, C.G. Nichols, Structure and dynamics of the pore of inwardly rectifying $K_{ATP}$ channels, Journal of Biological Chemistry 275 (2000) 1137–1144.
[26] J.F. Antcliff, S. Haider, P. Proks, M.S.P. Sansom, F.M. Ashcroft, Functional analysis of a structural model of the ATP-binding site of the $K_{ATP}$ channel Kir6.2 subunit, EMBO Journal 24 (2005) 229–239.
[27] F. Reimann, T.J. Ryder, S.J. Tucker, F.M. Ashcroft, The role of lysine 185 in the kir6.2 subunit of the ATP-sensitive channel in channel inhibition by ATP, Journal of Physiology (London) 520 (1999) 661–669.
[28] C.A. Cukras, I. Jeliazkova, C.G. Nichols, The role of NH2-terminal positive charges in the activity of inward rectifier $K_{ATP}$ channels, Journal of General Physiology 120 (2002) 437–446.
[29] S.A. John, J.N. Weiss, L. Xie, B. Ribalet, Molecular mechanism for ATP-dependent closure of the $K^+$ channel Kir6.2, Journal of Physiology (London) 552 (2003) 23–34.
[30] B. Ribalet, S.A. John, J.N. Weiss, Molecular basis for Kir6.2 channel inhibition by adenine nucleotides, Biophysical Journal 84 (2003) 266–276.
[31] A. Sali, T.L. Blundell, Comparative protein modelling by satisfaction of spatial restraints, Journal of Molecular Biology 234 (1993) 779–815.
[32] J.C. Phillips, R. Braun, W. Wang, J. Gumbart, E. Tajkhorshid, E. Villa, C. Chipot, R.D. Skeel, L. Kale, K. Schulten, Scalable molecular dynamics with NAMD, Journal of Computational Chemistry 26 (2005) 1781–1802.
[33] W. Humphrey, A. Dalke, K. Schulten, VMD — visual molecular dynamics, Journal of Molecular Graphics 14 (1996) 33–38.
[34] J. Ryckaert, A. Bellemans, G. Ciccotti, G.V. Paolini, Shear-rate dependence of the viscosity of simple fluids by nonequilibrium molecular dynamics, Physical Review Letters 60 (1988) 128–131.
[35] U. Essmann, L. Perera, M.L. Berkowitz, T. Darden, H. Lee, L. Pederson, A smooth particle mesh Ewald method, Journal of Chemical Physics 103 (1995) 8577–8593.
[36] D. Van Der Spoel, E. Lindahl, B. Hess, G. Groenhof, A.E. Mark, H.J. Berendsen, GROMACS: fast, flexible, and free, Journal of Computational Chemistry 26 (2005) 1701–1718.
[37] G.M. Morris, R. Huey, W. Lindstrom, M.F. Sanner, R.K. Belew, D.S. Goodsell, A.J. Olson, Autodock4 and autodocktools4: automated docking with selective receptor flexibility, Journal of Computational Chemistry 30 (2009) 2785–2791.
[38] D. Enkvetchakul, G. Loussouarn, E. Makhina, S.L. Shyng, C.G. Nichols, The kinetic and physical basis of $K_{ATP}$ channel gating: toward a unified molecular understanding, Biophysical Journal 78 (2000) 2334–2348.
[39] L. Li, J. Wang, P. Drain, The i182 region of Kir6.2 is closely associated with ligand binding in K(ATP) channel inhibition by ATP, Biophysical Journal 79 (2000) 841–852.
[40] P. Tammaro, C. Girard, J. Molnes, P.R. Njølstad, F.M. Ashcroft, Kir6.2 mutations causing neonatal diabetes provide new insights into Kir6.2-SUR1 interactions, EMBO Journal 24 (2005) 2318–2330.
[41] J. Aqvist, C. Medina, J.E. Samuelsson, A new method for predicting binding affinity in computer-aided drug design, Protein Engineering 7 (1994) 385–391.
[42] J. Aqvist, V.B. Luzhkov, B.O. Brandsdal, Ligand binding affinities from MD simulations, Accounts of Chemical Research 35 (2002) 358–365.
[43] T. Hansson, J. Marelius, J. Aqvist, Ligand binding affinity prediction by lineal interaction energy methods, Journal of Computer Aided Molecular Design 12 (1998) 27–35.
[44] W. Wang, J. Wang, P.A. Kollman, What determines the van der Waals coefficient beta in the LIE (linear interaction energy) method to estimate binding free energies using molecular dynamics simulations? Proteins 34 (1999) 395–402.
[45] Y.Y. Sham, Z.T. Chu, H. Tao, A. Warshel, Examining methods for calculations of binding free energies: LRA, LIE, PDLD-LRA, and PDLD/S-LRA calculations of ligands binding to an HIV protease, Proteins 39 (2000) 393–407.
[46] A. De Angeli, O. Moran, S. Wege, S. Filleur, G. Ephritikhine, S. Thomine, H. Barbier-Brygoo, F. Gambale, ATP binding to the C terminus of the *Arabidopsis thaliana* nitrate/proton antiporter, AtCLCa, regulates nitrate transport into plant vacuoles, Journal of Biological Chemistry 284 (2009) 26526–26532.
[47] M. Almlof, B.O. Brandsdal, J. Aqvist, Binding affinity prediction with different force fields: examination of the linear interaction energy method, Journal of Computational Chemistry 25 (2004) 1242–1254.
[48] P.A. Valiente, A. Gil, P.R. Batista, E.R. Caffarena, T. Pons, P.G. Pascutti, New parameterization approaches of the lie method to improve free energy calculations of PlmII-inhibitors complexes, Journal of Computational Chemistry 31 (2010) 2723–2734.
[49] A.M. Asi, N.A. Rahman, A.F. Merican, Application of the linear interaction energy method (LIE) to estimate the binding free energy values of *Escherichia coli* wild-type and mutant arginine repressor C-terminal domain (ArgRc)-L-arginine and ArgRc-L-citrulline protein–ligand complexes, Journal of Molecular Graphics and Modelling 22 (2004) 249–262.
[50] R. Zhou, R.A. Friesner, A. Ghosh, R.C. Rizzo, W.L. Jorgensen, M.R. Levy, New lineal interaction method for binding affinity calculations using a continuous solvent model, The Journal of Physical Chemistry. B 105 (2001) 10388–10397.
[51] J. Allen, Biophysical Chemistry, John Willey & Sons, Oxford, UK, 2008.
[52] D. Sheehan, Physical Biochemistry, John Willey & Sons, Oxford, UK, 2009.
[53] A. Kuo, J.M. Gulbis, J.F. Antcliff, T. Rahman, E.D. Lowe, J. Zimmer, J. Cuthbertson, F.M. Ashcroft, T. Ezaki, D.A. Doyle, Crystal structure of the potassium channel KirBac1.1 in the closed state, Science 300 (2003) 1922–1926.
[54] M. Nishida, R. MacKinnon, Structural basis of inward rectification: cytoplasmic pore of the g protein-gated inward rectifier girk1 at 1.8 Å resolution, Cell 111 (2002) 957–965.
[55] X. Tao, J.L. Avalos, J. Chen, R. MacKinnon, Crystal structure of the eukaryotic strong inward-rectifier $K^+$ channel Kir2.2 at 3.1 Å resolution, Science 326 (2009) 1668–1674.
[56] M. Nishida, M. Cadene, B.T. Chait, R. MacKinnon, Crystal structure of a Kir3.1-prokaryotic Kir channel chimera, EMBO Journal 26 (2007) 4005–4015.
[57] J. Krumrine, F. Raubacker, N. Brooijmans, I. Kuntz, Principles and methods of docking and ligand design, in: P.E. Bourne, H. Weissig (Eds.), Structural Bioinformatics, 2003, pp. 443–476.
[58] N. Brooijmans, I.D. Kuntz, Molecular recognition and docking algorithms, Annual Review of Biophysics and Biomolecular Structure 32 (2003) 335–373.
[59] M. Takano, L.H. Xie, H. Otani, M. Horie, Cytoplasmic terminus domains of Kir6.x confer different nucleotide-dependent gating on the ATP-sensitive $K^+$ channel, The Journal of Physiology 512 (1998) 395–406.
[60] S.L. Shyng, C.A. Cukras, J. Harwood, C.G. Nichols, Structural determinants of $PIP_2$ regulation of inward rectifier $K_{ATP}$ channels, Journal of General Physiology 116 (2000) 599–608.